DOI: 10.1002/ejic.200600894

The Synthesis, Crystal and Band Structures, and Properties of the Quaternary Supramolecular Complexes $[Hg_6Z_4](MX_6)Hg_y$ (Z = As, Sb; M = Hg, Cd; X = Cl, Br, I; y = 0, 0.5, 0.6)

Jian-Ping Zou,[a,b] Yan Li,[a] Ming-Lai Fu,[a] Guo-Cong Guo,*[a] Gang Xu,[a] Xue-Hui Liu,[a] Wei-Wei Zhou,[a] and Jin-Shun Huang[a]

Keywords: Density functional calculations / Host–guest systems / Pnictides / Semiconductors / Supramolecular chemistry

The series of supramolecular complexes $(Hg_6As_4)(CdCl_6)Hg_{0.5}$ (**1**), $(Hg_6As_4)(HgCl_6)Hg_{0.5}$ (**2**), $(Hg_6As_4)(CdBr_6)$ (**3**), and $(Hg_6Sb_4)(CdI_6)Hg_{0.6}$ (**4**) has been prepared by a solid-state reaction and their crystal structures determined by single-crystal X-ray diffraction. All these compounds crystallize in the space group $Pa\bar{3}$ with four formula units in a cell: a = 12.172(2) (**1**), 12.189(1) (**2**), 12.3738(5) (**3**), and 13.234(2) Å (**4**). Their structures feature a 3D cationic host framework that is built up of linearly coordinated mercury and tetrahedrally coordinated pnicogen atoms to form distorted As_2Hg_6 or Sb_2Hg_6 octahedra, and discrete guest anions. The distorted octahedra corner-share with each other to form a perovskite-like, 3D cationic framework that possess two types of closed cavities with different sizes. The octahedral guest anions $(MX_6)^{4-}$ are embedded in the larger cavities, whereas the smaller cavities trap the excess mercury atoms or remain empty. The optical properties were investigated by diffuse reflectance and FT IR spectroscopy. The electronic band structures and density of states (DOS) calculated by DFT methods indicate that the present compounds are semiconductors and that the optical absorption mainly originates from the charge transitions from the p orbital of the pnicogen (As or Sb) and halogen (Cl, Br or I) atoms states to the Hg1 6s states for **1**, **3**, and **4**, and to Hg1 6s and Hg3 6s states for **2**.

Introduction

The field of inorganic supramolecular chemistry has attracted more and more attention and has experienced enormous growth because it covers a large diversity of compounds that possess a huge variety of crystal and electronic structures and physical and chemical properties.[1] For instance, a broad family of supramolecular assemblies based on mercury pnicogen cationic frameworks has been reported since the 1990s.[2] Among them, the three dimensional host frameworks with positive charges are ordinarily built up of linearly coordinated mercury and tetrahedrally coordinated pnicogen atoms, whereas the guest anions are usually composed of halometalate or monoatomic anions with different shapes and sizes.[3] Two principal types of networks can be distinguished in these compounds according to the dimensions of the voids. The first type are analogues of the well-known Millon's base salts,[4] which are composed of cationic frameworks with the formula $(Hg_2Z)^+$ (Z = P, As) and adopt a tridymite-like topology filled with different tetrahedral anions such as ZnI_4^{2-}[3c,3d] or CdI_4^{2-}.[3g] The second one is the topology with the formula $(Hg_6Z_4)^{4+}$ (Z = P, As, Sb),[3,5] among which the frameworks possess cavities of two different sizes in close proximity. These are capable of trapping guests of two different types: octahedral guests with the formula $(MX_6)^{4-}$ or $(M'X_6)^{3-}$ (M = divalent metal atoms; M′ = trivalent metal atoms; X = Cl, Br, I)[2b,2c,3] in the bigger cavities and monoatomic guests in the smaller ones. In most cases, the coordination centers of the octahedral guests are trivalent metal atoms rather than divalent metal atoms. Until now, two divalent metals, namely Hg[3b,6] and Fe,[2b] acting as the coordination centers of the octahedral guest anions have been reported, among which only one quaternary supramolecular mercury pnictide halide, $(Hg_4As_6)(FeBr_6)Hg_{0.6}$,[2b] has been characterized.

Recently, we have begun a systematic investigation of mercury pnictide-based mixed-framework compounds to further explore new self-assembly supramolecular materials. The idea is to exploit cationic host framework that have various structures together with different cavities for trapping different guest anions. Because the II–V group compounds have good semiconducting and thermoelectric properties,[7] we have chosen mercury and cadmium in combination with pnicogens in order to obtain new semicon-

[a] State Key Laboratory of Structural Chemistry, Fujian Institute of Research on the Structure of Matter, Chinese Academy of Sciences,
Fuzhou, Fujian 350002, P. R. China
Fax: +86-591-8371-4946
E-mail: gcguo@ms.fjirsm.ac.cn
[b] Graduate School, Chinese Academy of Sciences,
Beijing 100039, P. R. China
Supporting information for this article is available on the WWW under http://www.eurjic.org or from the authors.

ducting compounds with unique physical properties and abundant structural features. Our ongoing research in this field has resulted in some interesting compounds.[2e,3g]

In the present work, with the intention of preparing new quaternary host–guest compounds based on the mercury-pnicogen framework, we selected divalent cadmium cation as the coordination center of the octahedral guest anions and changed the halogen and pnicogen atoms from Cl to I, and P to Sb, respectively. We succeeded in synthesizing a new series of supramolecular complexes, $(Hg_6As_4)(CdCl_6)$-$Hg_{0.5}$ (**1**), $(Hg_6As_4)(HgCl_6)Hg_{0.5}$ (**2**), $(Hg_6As_4)(CdBr_6)$ (**3**), and $(Hg_6Sb_4)(CdI_6)Hg_{0.6}$ (**4**). Herein, we report the syntheses, crystal and band structures, and properties of these new supramolecular inorganic complexes. These band structure and optical and thermal studies are the first to be reported for supramolecular complexes based on mercury pnictide halides, which are also the major interest for us.

Results and Discussion

The present compounds are all stable in air. Their crystal structures were determined by means of single-crystal X-ray diffraction. All these compounds have a similar structural organization. Their crystal structures feature a 3D cationic host framework and discrete different guest anions. The 3D cationic network is built up of linearly coordinated mercury and tetrahedrally coordinated pnicogen atoms to form distorted As_2Hg_6 or Sb_2Hg_6 octahedra. The distorted octahedra corner-share with each other to form a perovskite-like 3D cationic framework that possess two types of closed cavities with different sizes (Figure 1).

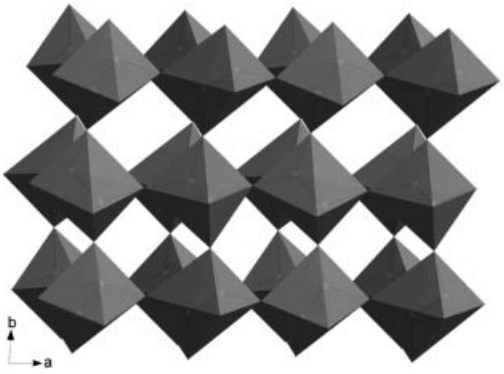

Figure 1. The perovskite-like 3D cationic framework built from corner-sharing distorted octahedra viewed along the *c* axis.

The octahedral guest anions $(CdCl_6)^{4-}$, $(HgCl_6)^{4-}$, and $(CdI_6)^{4-}$ are embedded in the larger cavities of the host framework in **1**, **2**, and **4**, respectively, whereas the smaller cavities trap the excess mercury atoms with 50%, 50%, and 60% site occupancy for **1**, **2**, and **4**, respectively (Figure 2). Partial occupancy of the smaller cavities by mercury atoms has been reported previously in the literature, particularly for $(Hg_6As_4)(HgCl_6)Hg_{0.4}$, which is nearly same as **2** except for the different occupancy of the discrete mercury atom.[2b,3b] Like the ternary compounds $(Hg_6P_4)(HgBr_6)$[3b] and $(Hg_6Sb_4)(HgBr_6)$,[6a] in which the larger cavities of the host framework are filled with the octahedral guest anions $(HgX_6)^{4-}$ with the smaller cavities remaining empty, compound **3** is the first quaternary compound with this structural feature in metal pnictide halides (see Figure S1 in the Supporting Information).

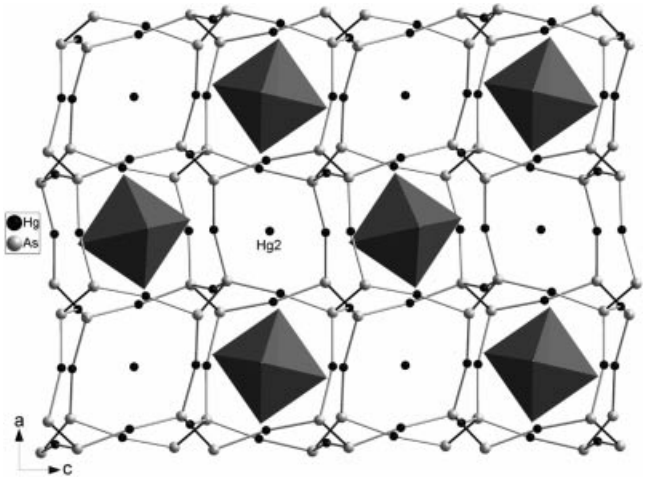

Figure 2. View of the structure of **1**, **2**, and **4** along the *b* axis. The $(CdCl_6)^{4-}$, $(HgCl_6)^{4-}$, and $(CdI_6)^{4-}$ octahedra are drawn in grey.

The Hg1–As, Hg1–Sb, and As–As bond lengths in the cationic moieties in the present compounds range from 2.496(2) to 2.531(2), 2.686(2) to 2.693(2), and 2.389(7) to 2.428(6) Å, respectively, all of which lie in the normal ranges for Hg–Z and As–As bond lengths in known mercury pnictide halides.[2–6] The Sb–Sb bond length of 2.790(5) Å is also in good agreement with those found in various mercury antimonide halides.[3f,6a] The Hg3–Cl [2.70(1) Å] and Cd–X [Cd–Cl 2.636(7), Cd–Br 2.806(3), Cd–I 3.006(2) Å] bond lengths in the guest anions are all close to the those in mercury and cadmium pnictide halides.[2e,2f]

The distances between the hosts and anionic guests in the present compounds are significantly longer than the expected values for covalent bonding, thus suggesting the typical supramolecular interactions between them.[1b] The interatomic distance between the chlorine atoms of the guest anions and the mercury atoms in the host framework range from 2.95 to 3.30, 2.93 to 3.30, 3.02 to 3.28, and 3.20 to 3.58 Å for **1**, **2**, **3**, and **4**, respectively, all of which are much longer than the Hg–X covalent bond lengths but shorter than the sum of the van der Waals radii of Hg and X. Therefore, host–guest supramolecular interactions are present in the crystal structures and these fix the octahedral guest anions to their specific positions so that no positional or rotational disorder is observed. This situation has also been reported in the literature.[2b,2d,2h]

As for the monatomic guests, the discrete mercury atoms have similar environments in **1**, **2**, and **4**. In the first coordination sphere, each Hg atom displays a coordination number of 14 [(6 Hg + 2 As + 6 Cl) in **1** and **2** and (6 Hg + 6 I + 2 Sb) in **4**]. The distances between the hosts and monatomic guests fall in the ranges 3.50–3.68 Å for **1**, 3.55–3.70 Å for **2**, and 3.68–3.92 Å for **4**. With such coordination, the monatomic guests can be regarded as being clath-

rated with an oxidation state of zero, similar to the case found in $(Hg_6As_4)(HgCl_6)Hg_{0.4}$[3b] and $(Hg_6As_4)(FeBr_6)$-$Hg_{0.6}$,[2b] where the zero oxidation state of the guest mercury was confirmed by means of solid-state ^{199}Hg NMR spectroscopy.

As shown in Figure 3, the diffuse reflectance spectra of the present compounds reveal the presence of an optical gap of 2.05, 2.01, 1.94, and 1.23 eV for **1**–**4**, respectively, which suggests that the compounds are semiconductors and is consistent with their colors. The bandgaps are shifted to lower energies in the order Cl > Br > I, which is similar to other cases reported in the literature.[8] The bandgap of **4** is close to those of CdTe (1.44 eV), GaAs (1.43 eV), and $CuInS_2$ (1.55 eV), all of which are highly efficient photovoltaic materials.[9] Thus, we suppose that this compound may find a use for the efficient absorption of solar radiation in solar cell applications. The IR spectra of the present compounds show no obvious absorptions in the range of 4000–400 cm^{-1} (see Figures S2–S5 in the Supporting Information) which, in combination with their good thermal stability (see Figure S6–S9 in the Supporting Information), may make them useful as window materials for laser delivery media and infrared transmitters for optical fiber applications in telecommunications.[10]

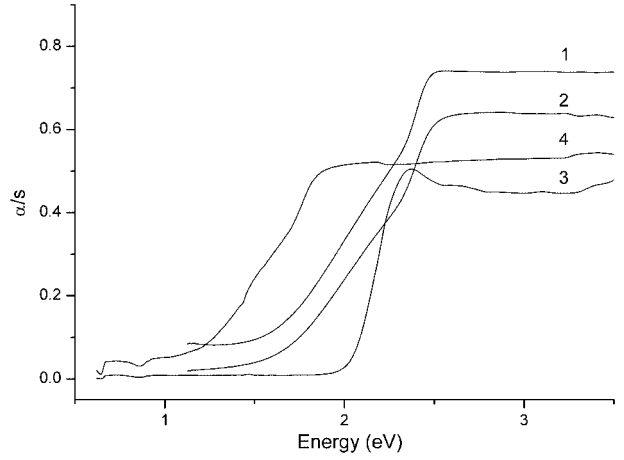

Figure 3. Diffuse reflectance spectra of **1**–**4**.

The calculated band structures of the present compounds along the high symmetry points of the first Brillouin zone are plotted in Figure 4a–d for **1**–**4**, respectively. It can be seen that the valence bands (VBs) and conduction bands (CBs) are both disperse. All four compounds show semiconductor character: the lowest *k*-point of the CBs and the highest *k*-point of the VBs are both localized at the G point and the direct bandgaps are about 1.86, 1.72, and 1.89 eV for **1**–**3**, respectively. For **4**, the lowest *k*-point of the CBs and the highest *k*-point of the VBs are not localized at the same point, which indicates that compound **4** has indirect semiconductor character, with a bandgap of 1.33 eV. The calculated energy gaps for the present compounds are similar to their experimental values. The bands can be assigned according to total and partial densities of states (DOS), as plotted in parts a–d of Figure 5 for **1**–**4**, respectively. In **1**

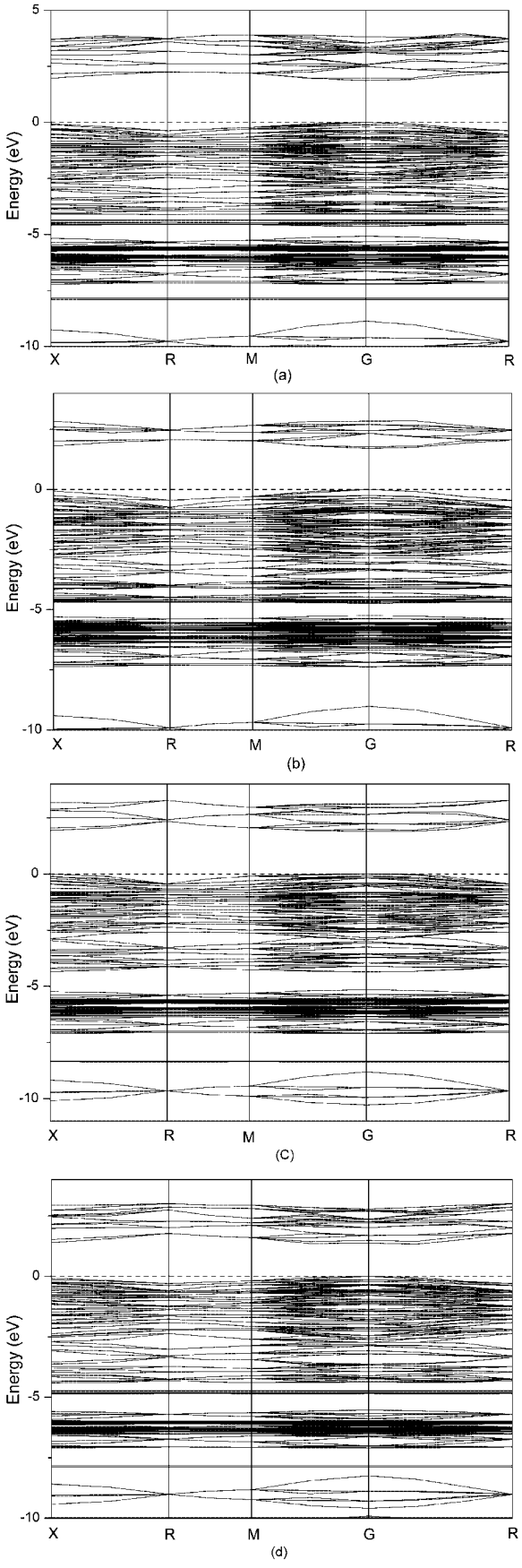

Figure 4. The band structures of **1** (a), **2** (b), **3** (c), and **4** (d). The Fermi level is set at 0 eV.

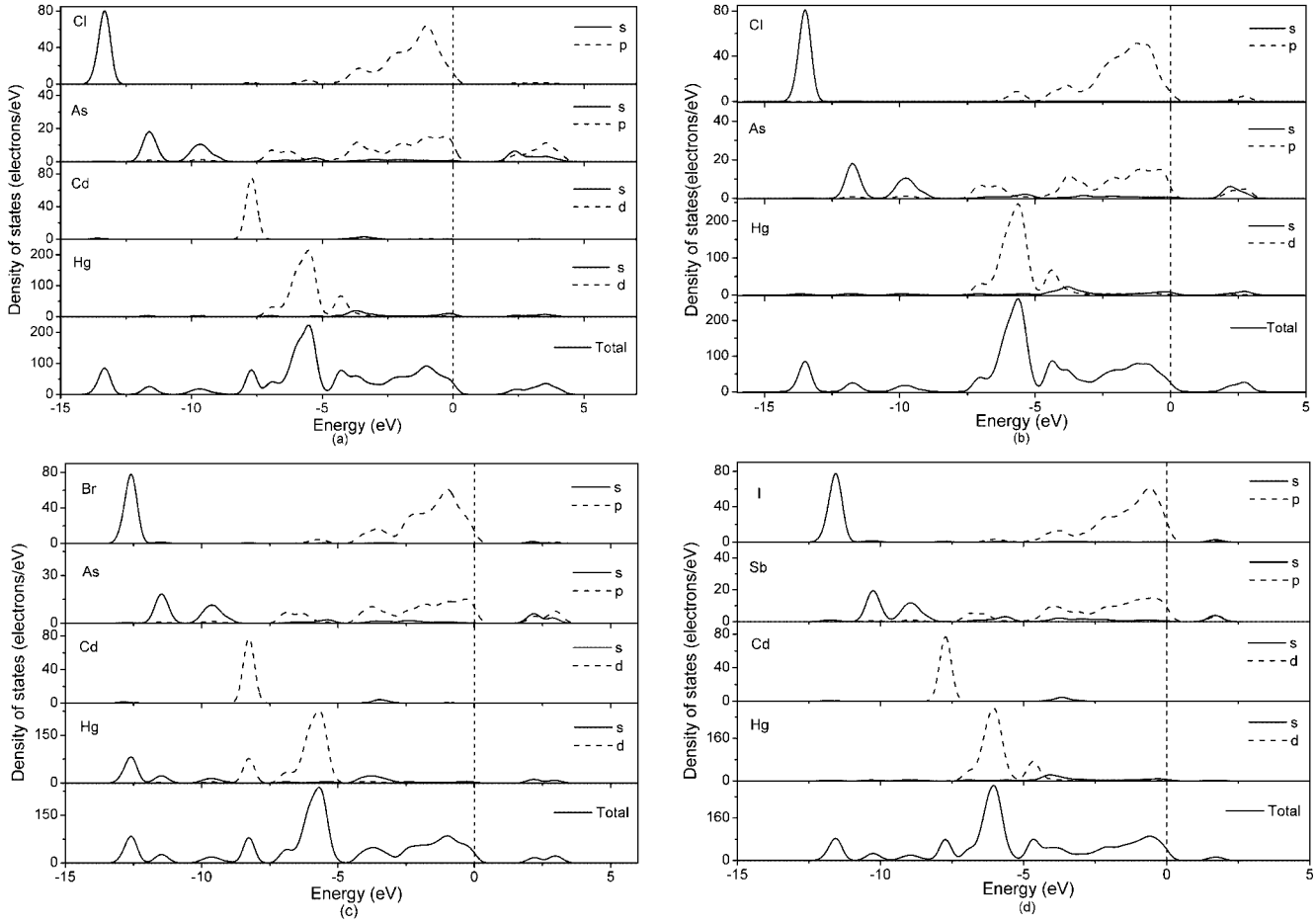

Figure 5. Total and partial density of states for **1** (a), **2** (b), **3** (c), and **4** (d). The Fermi level (vertical dotted line) is set at 0 eV.

and **2**, the VBs between –15.0 and –5.0 eV are mostly formed by the Hg 5d and Cd 4d states mixing with small Cl 3s and As 4s states, and the VBs lying about between –5.0 eV and the Fermi level (0.0 eV) are the main contributions from the Cl 3p and As 4p states mixing with a small amount of Hg 5d state, while the CBs between 1.7 and 5.0 eV are due to the Hg 6s, As 4s, and As 4p states. In addition, comparing the partial DOS of the different types of mercury atoms in **1** and **2** (parts a,b in Figure 6), the DOS of Hg1 6s state is seen to be much higher than that of the Hg2 6s state at the bottom of the CBs in **1**, and the DOS of the Hg1 6s and Hg3 6s states are much higher than that of the Hg2 6s state at the bottom of the CBs in **2**. This shows that electron transitions mostly come from the s orbital of the mercury atoms in the host framework or the octahedral guest anions rather than from the s orbital of the monoatomic mercury to Cl 3p and As 4p states. Therefore, the optical absorption is mainly ascribed to the charge transitions from Cl 3p and As 4p to Hg1 6s states for **1**, and Cl 3p and As 4p to Hg1 6s and Hg3 6s states for **2**.

Similarly, the VBs between –15.0 and –5.0 eV are mostly formed by the Hg 5d and Cd 4d states mixing with small Br 4s, As 4s, and Hg 6s, and I 5s and Sb-5s states for **3** and **4**, respectively. The VBs between –5.0 eV and the Fermi level (0.0 eV) are mostly formed by Br 4p and As 4p states for **3**, and I 5p and Sb 5p states for **4**, hybridized with a small amount of the s orbital of the transition metals, whereas the CBs between 1.3 and 5.0 eV are made from the Hg 6s state mixed with the s and p orbitals of the pnicogen atoms. Thus, it can be concluded that the optical absorption can be mainly assigned to the charge transitions from Br 4p and As 4p to Hg 6s states for **3**. As shown in Figure 6 (c), the partial DOS of the different type of mercury atoms in **4** shows that the DOS of the Hg1 6s state is much higher than that of the Hg2 6s state at the bottom of the CBs, which indicates that the electron transitions arise mostly from the Hg1 6s rather than Hg2 6s to I 5p and Sb 5p states. Therefore, the optical absorption is mainly ascribed to the charge transitions from I 5p and Sb 5p to Hg1 6s.

In addition, we calculated the atomic site and angular momentum projected DOS of the present compounds to elucidate the nature of the electronic band structures and chemical bonds. As shown in Figure 5, we observed that the density and shape of the p orbital of the pnicogen atoms states are similar to that of the Hg 6s state between –5.0 and –2.5 eV, while the DOS of the p orbital of the halogen atoms states are higher than that of the Cd 5s state (Hg 6s state for **2**) for each compound. Accordingly, we can conclude that there are strongly covalent Hg1–As and Hg1–Sb

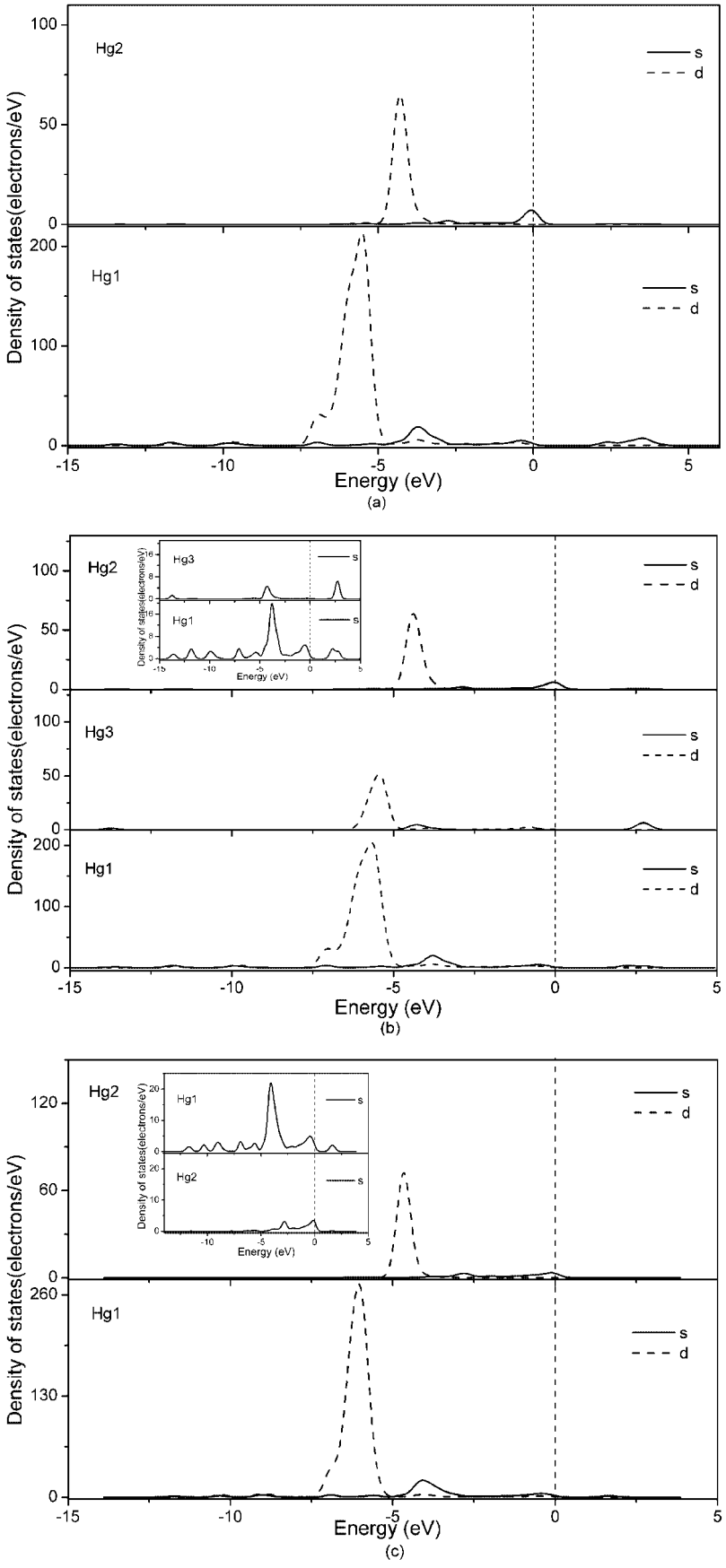

Figure 6. Partial density of states of the Hg atoms in **1** (a), **2** (b), and **4** (c). The Fermi level (vertical dotted line) is set at 0 eV. The insets show an expansion of the low-energy region for Hg1 and Hg3 in (b) and Hg1 and Hg2 in (c).

interactions in the host cations and weakly covalent Cd–Cl, Hg3–Cl, Cd–Br, and Cd–I interactions in the guest anions for **1**–**4**, respectively.

Semi-empirical population analyses allow for a more quantitative bond analyses. The calculated bond orders of **1**–**4** within a unit cell are listed in Table 1; the bond order of a purely covalent single bond is generally 1.0 e. As can be seen, except for the Z–Z bond in **4**, the covalent interactions of the bonds are in the order Hg1–X < M–X < Z–Z < Hg1–Z (M = Hg3 for **2** and Cd for **1**, **3**, **4**) for each compound. This indicates that the covalent interactions of the Hg–Z bonds are stronger than those of the M–X bonds, which is in agreement with the results from the DOS analyses. The Hg1–X bond is the weakest of all four types of bonds, which is consistent with the existence of supramolecular interactions between the host framework and guest anions.

Table 1. Calculated bond orders (e) of **1**–**4** within the unit cell.

	Hg1–Z	Z–Z	M–X[a]	Hg1–X
1	0.48 to 0.49	0.36	0.29	0.04 to 0.16
2	0.47 to 0.48	0.34	0.26	0.04 to 0.16
3	0.54 to 0.62	0.45	0.26	–0.18 to –0.02
4	0.59 to 0.75	0.77	0.12	–0.42 to –0.22

[a] M = Hg3 for **2** and Cd for **1**, **3**, and **4**.

Conclusions

In summary, a series of quaternary supramolecular $[Hg_6Z_4](MX_6)Hg_y$ complexes has been synthesized and structurally characterized. Their main structural feature is that they all consist of discrete guest anions and a perovskite-like 3D cationic framework composed of corner-sharing distorted As_2Hg_6 or Sb_2Hg_6 octahedra that possesses two types of closed cavities with different sizes. The octahedral guest anions $(MX_6)^{4-}$ are embedded in the larger cavities, while the smaller cavities trap the excess mercury atoms or remain empty. The present compounds, which have a bandgap range of 1.2–2.1 eV and are transparent over a broad range of IR frequencies, may have applications as efficient photovoltaic materials and IR window materials. The calculations of the electronic band structures and density of states (DOS) indicate that their optical absorption mainly originates from the charge transitions from the p orbital of the pnicogen and halogen atoms to the Hg1 6s states for **1**, **3**, and **4**, and to Hg1 6s and Hg3 6s for **2**.

Experimental Section

Materials and Measurement: All chemicals were analytically pure (>99.99%) and used without further purification. The powder X-ray diffraction patterns were collected with a Rigaku DMAX2500 diffractometer at 40 kV and 100 mA for Cu-K_α radiation (λ = 1.5406 Å) with a scan speed of 5° per minute at room temperature. The simulated patterns were produced using the Mercury program and single-crystal reflection data. Thermogravimetric analysis (TGA) and differential scanning calorimetry were performed on a Netzsch Sta449C thermoanalyzer under a N_2 atmosphere in the range 30–800 °C at a heating rate of 10 °C min^{-1}. IR spectra were recorded with a Magna 750 FT-IR spectrometer as KBr pellets in the range 4000–400 cm^{-1}. Optical diffuse reflectance spectra were measured with a PE Lambda 35 UV/Vis spectrophotometer for **1** and **2**, and a 900 UV/Vis spectrophotometer for **3** and **4** equipped with an integrating sphere at 293 K, and the $BaSO_4$ plate was used as the reference. The absorption spectra were calculated from reflection spectra by the Kubelka–Munk function:[11] $\alpha/S = (1 - R)^2/2R$, where α is the absorption coefficient, S is the scattering coefficient, which is practically wavelength independent when the particle size is larger than 5 μm, and R is the reflectance. The energy gap was determined as the intersection point between the energy axis at the absorption offset and the line extrapolated from the linear portion of the absorption edge in the α/S vs. E (eV) plot. Microprobe elemental analysis on Hg, Cd, Sb, As, Cl, Br, and I for the present compounds were performed with a field-emission scanning electron microscope (FESEM, JSM6700F) equipped with an energy dispersive X-ray spectroscope (EDS, Oxford INCA).

Synthesis of $(Hg_6As_4)(CdCl_6)Hg_{0.5}$ (1): Yellow crystals of **1** were initially prepared by the solid-state reaction of a mixture of $HgCl_2$ (1.5 mmol, 407 mg), Cd (0.5 mmol, 56 mg), $CdCl_2$ (0.5 mmol, 91 mg), and As (1.0 mmol, 75 mg) at 450 °C for 120 h. Microscope element analysis on several single crystals of **1** confirmed the presence of Hg, Cd, As, and Cl in the approximate molar ratio 6.5:1.0:3.9:6.1, which is in good agreement with that obtained from structural analysis. After structural analysis, a yellow crystalline sample of **1** was obtained quantitatively by the reaction of a mixture of Hg_2Cl_2, Hg, Cd, and As in a 6:1:2:8 molar ratio at 450 °C for 120 h. The TGA curve of **1** shows no weight change up to 310 °C (see Figure S6 in the Supporting Information). The purity of the yellow crystalline sample was confirmed by XRD powder diffraction (see Figure S10 in the Supporting Information). The powder diagram of **1** shows some splitting of the reflections, which indicates there is a lower symmetry in **1**.

Synthesis of $(Hg_6As_4)(HgCl_6)Hg_{0.5}$ (2): Yellow crystals of **2** were initially prepared by the reaction of a mixture of Hg_2Cl_2 (1.0 mmol, 472 mg), Cd (0.5 mmol, 56 mg), and As (1.0 mmol, 75 mg) at 320 °C for 120 h in an attempt to obtain the new phase $(Hg_6As_4)(CdCl_6)$. The results of the single-crystal X-ray diffraction analysis indicated the absence of Cd. Microscope element analysis on several single crystals of **2** confirmed the presence of Hg, As, and Cl in the approximate molar ratio 7.4:4.0:5.9, which is in good agreement with that obtained from structural analysis. After structural analysis, a yellow crystalline sample of **2** was then obtained quantitatively by the reaction of a mixture of Hg_2Cl_2, Hg, and As in a 6:3:8 molar ratio at 320 °C for 120 h. The TGA curve of **2** shows no weight change up to 320 °C (see Figure S7 in the Supporting Information). The purity of the yellow crystalline sample was confirmed by XRD powder diffraction (see Figure S11 in the Supporting Information). The powder diagram of **2** shows some splitting of the reflections, which indicates there is a lower symmetry in **2**.

Synthesis of $(Hg_6As_4)(CdBr_6)$ (3): Red crystals of **3** were prepared by the reaction of a mixture of $HgBr_2$ (1.0 mmol, 361 mg), Cd (0.5 mmol, 56 mg), and As (1.0 mmol, 75 mg) at 350 °C for 120 h. Microscope element analysis on several single crystals of **3** confirmed the presence of Hg, Cd, As, and Br in the approximate molar ratio 5.9:1.0:3.9:5.8, which is in good agreement with that obtained from structural analysis. After structural analysis, a red crystalline sample of **3** was then obtained quantitatively by the reaction of a mixture of Hg_2Br_2, Cd, and As in a 3:1:4 molar ratio at 350 °C for 120 h. The TGA curve of **3** shows no weight change up to

Table 2. Crystal data and structure refinement parameters for **1**, **2**, **3**, and **4**.

	1	**2**	**3**	**4**
Empirical formula	$[Hg_6As_4](CdCl_6)Hg_{0.5}$	$[Hg_6As_4](HgCl_6)Hg_{0.5}$	$[Hg_6As_4](CdBr_6)$	$[Hg_6Sb_4](CdI_6)Hg_{0.6}$
Formula mass [g mol^{-1}]	1928.61	2016.80	2095.08	2684.69
Crystal color	yellow	yellow	red	black
Crystal habit	plate	plate	chip	block
Crystal system	cubic	cubic	cubic	cubic
Space group	$Pa\bar{3}$	$Pa\bar{3}$	$Pa\bar{3}$	$Pa\bar{3}$
a [Å]	12.172(2)	12.189(1)	12.3738(5)	13.234(2)
Volume [Å^3]	1803.2(5)	1810.7(3)	1894.6(1)	2317.7(7)
Z	4	4	4	4
λ (Mo-K_α) [Å]	0.71073	0.71073	0.71073	0.71073
$D_{calcd.}$ [g cm^{-3}]	7.104	7.398	7.345	7.694
μ [mm^{-1}]	64.427	71.452	69.095	56.981
$F(000)$	3208	3336	3480	4392
θ range [°]	2.90–25.03	2.89–25.06	3.68–25.09	2.67–25.02
Reflections collected	604	628	11390	2174
Observed reflections	377	380	421	445
Independent reflections	534	546	554	683
R_1,[a] wR_2[b]	0.0499, 0.1052	0.0666, 0.1570	0.0565, 0.0963	0.0646, 0.1104
Goodness-of-fit	0.998	0.999	0.990	0.994
$\Delta\rho_{max}$ and $\Delta\rho_{min}$ [e/Å^3]	2.457, –2.905	3.959, –4.863	3.200, –2.611	3.295, –2.702

[a] $R = \Sigma||F_o| - |F_c||/\Sigma|F_o|$. [b] $R_w = \{\Sigma[w(F_o^2 - F_c^2)^2]/\Sigma[w(F_o^2)^2]\}^{1/2}$.

Table 3. Selected bond lengths [Å] and angles [°] for **1**–**4**.[a]

Compound **1**			
Hg(1)–As(1)	2.496(2)	Cd(1)–Cl(1) × 6	2.636(7)
Hg(1)–As(2)	2.498(2)	As(1)–As(2) × 2	2.392(6)
Hg(1)–Cl(1)	2.947(6)		
As(1)–Hg(1)–As(2)	164.3(1)	As(2)#3–As(1)–Hg(1)	106.5(1)
As(1)–Hg(1)–Cl(1)	106.3(2)	Hg(1)–As(1)–Hg(1)#4	112.24(9)
As(2)–Hg(1)–Cl(1)	87.2(2)	As(1)#5–As(2)–Hg(1)	110.47(9)
Cl(1)#1–Cd(1)–Cl(1)#2	93.1(2)	Hg(1)–As(2)–Hg(1)#6	108.5(1)
Cl(1)#1–Cd(1)–Cl(1)	86.9(2)	Cd(1)–Cl(1)–Hg(1)	100.2(2)
Cl(1)#2–Cd(1)–Cl(1)	180.0(3)		
Compound **2**			
Hg(1)–As(1)	2.496(2)	Hg(3)–Cl(1) × 6	2.701(1)
Hg(1)–As(2)	2.502(2)	As(1)–As(2) × 2	2.389(7)
Hg(1)–Cl(1)	2.933(9)		
As(1)–Hg(1)–As(2)	164.4(1)	Cl(1)#1–Hg(3)–Cl(1)#4	180.0
As(1)–Hg(1)–Cl(1)	106.3(2)	As(2)#5–As(1)–Hg(1)	106.8(1)
As(2)–Hg(1)–Cl(1)	87.1(2)	Hg(1)#6–As(1)–Hg(1)	111.98(11)
Cl(1)#1–Hg(3)–Cl(1)#2	86.6(2)	As(1)#7–As(2)–Hg(1)	110.3(1)
Cl(1)#2–Hg(3)–Cl(1)	93.4(2)	Hg(1)–As(2)–Hg(1)#8	108.6(1)
Cl(1)–Hg(3)–Cl(1)#3	180.0(4)	Hg(3)–Cl(1)–Hg(1)	99.6(3)
Compound **3**			
Hg(1)–As(2)	2.529(2)	Cd(1)–Br(1) × 6	2.806(3)
Hg(1)–As(1)	2.531(2)	As(1)–As(2) × 2	2.428(6)
Hg(1)–Br(1)	3.022(3)		
As(2)–Hg(1)–As(1)	165.5(1)	Br(1)#1–Cd(1)–Br(1)	180.0(1)
As(2)–Hg(1)–Br(1)	87.31(8)	Cd(1)–Br(1)–Hg(1)	98.34(9)
As(1)–Hg(1)–Br(1)	105.2(1)	As(2)#4–As(1)–Hg(1)#5	107.3(1)
Br(1)#1–Cd(1)–Br(1)#2	86.67(8)	Hg(1)#5–As(1)–Hg(1)#6	111.6(1)
Br(1)#1–Cd(1)–Br(1)#3	93.33(7)	As(1)#7–As(2)–Hg(1)	110.5(1)
Br(1)#2–Cd(1)–Br(1)#3	86.67(7)	Hg(1)#8–As(2)–Hg(1)	108.5(1)
Compound **4**			
Hg(1)–Sb(2)	2.686(2)	Cd(1)–I(1) × 6	3.006(2)
Hg(1)–Sb(1)	2.693(2)	Sb(1)–Sb(2) × 2	2.790(5)
Hg(1)–I(1)	3.204(3)		
Sb(2)–Hg(1)–Sb(1)	161.92(9)	I(1)–Cd(1)–I(1)#2	180.0
Sb(2)–Hg(1)–I(1)	85.22(7)	Hg(1)#3–Sb(1)–Hg(1)	112.75(7)
Sb(1)–Hg(1)–I(1)	108.54(8)	Hg(1)#3–Sb(1)–Sb(2)#4	105.95(8)
I(1)#1–Cd(1)–I(1)	87.33(5)	Hg(1)–Sb(2)–Hg(1)#5	110.79(7)
I(1)#1–Cd(1)–I(1)#2	92.67(5)	Hg(1)–Sb(2)–Sb(1)#6	108.11(7)

[a] Symmetry transformations used to generate equivalent atoms. **1**: #1 –*y* + 1/2, *z* + 1/2, *x*; #2 –*x*, –*y* + 1, –*z*; #3 –*x* + 1/2, *y* + 1/2, *z*; #4 –*y* + 1, *z* + 1/2, –*x* + 1/2; #5 –*x* + 1/2, *y* – 1/2, *z*; #6 *z*, *x*, *y*. **2**: #1 –*y* + 1, –*z*, –*x* + 1; #2 *z* + 1, *x* – 1, *y*; #3 –*x* + 2, –*y*, –*z*; #4 *y* + 1, *z*, *x* – 1; #5 –*x* + 3/2, *y* – 1/2, *z*; #6 *z* + 1/2, –*x* + 1/2, –*y*; #7 –*x* + 3/2, *y* + 1/2, *z*; #8 –*z* + 1, *x* – 1/2, –*y* + 1/2. **3**: #1 –*x*, –*y* + 1, –*z* + 1; #2 –*y* + 1/2, –*z* + 1, *x* + 1/2; #3 –*z* + 1/2, *x* + 1/2, *y*; #4 *x* – 1/2, *y*, –*z* + 1/2; #5 –*z*, *x* + 1/2, –*y* + 1/2; #6 *y* – 1/2, –*z* + 1/2, –*x*; #7 *x* + 1/2, *y*, –*z* + 1/2; #8 *y*, *z*, *x*. **4**: #1 –*y* + 1, –*z* + 1, –*x* + 1; #2 –*x* + 1, –*y* + 1, –*z* + 1; #3 –*y* + 1/2, –*z* + 1, *x* + 1/2; #4 –*x* + 1/2, *y* – 1/2, *z*; #5 –*z* + 1, *x* + 1/2, –*y* + 3/2; #6 –*x* + 1/2, *y* + 1/2, *z*.

280 °C (see Figure S8 in the Supporting Information). The purity of the red crystalline sample was confirmed by XRD powder diffraction (see Figure S12 in the Supporting Information).

Synthesis of $(Hg_6Sb_4)(CdI_6)Hg_{0.6}$ (4): Black crystals of **4** were prepared by the reaction of a mixture of Hg_2I_2 (0.6 mmol, 393 mg), Cd (0.3 mmol, 34 mg), and Sb (0.9 mmol, 110 mg) at 350 °C for 120 h. Microscope element analysis on several single crystals of **4** confirmed the presence of Hg, Cd, Sb, and I in the approximate molar ratio 6.5:1.0:4.2:6.1, which is in good agreement with that obtained from structural analysis. After structural analysis, a mixture of liquid mercury and a black crystalline sample of **4** was then obtained quantitatively by the reaction of a mixture of Hg_2I_2, Hg, Cd, and Sb in a 3:1:1:4 molar ratio at 350 °C for 120 h. The TGA curve of **4** shows no weight change up tol 260 °C (see Figure S9 in the Supporting Information). The purity of the black crystalline sample was confirmed by XRD powder diffraction (see Figure S13 in the Supporting Information).

X-ray Crystallographic Studies: Single crystals of **1**–**4** suitable for X-ray analysis were mounted at the apex of a glass fiber for data collection. Data sets for **1**, **2**, and **4** were collected with a Rigaku AFC7R diffractometer, and that for **3** was collected with Rigaku Mercury CCD, both of which were equipped with a graphite-monochromated Mo-K_α radiation source (λ = 0.71073 Å) from a rotating anode generator at 293 K. The intensity data were collected with the ω-scan technique and corrected for Lorentz polarization factors. All the structures were solved by direct methods and difference Fourier synthesis and refined by full-matrix least-squares techniques using the Siemens SHELXTL™ version 5 crystallographic software package.[12] All atoms were refined anisotropically. Crystallographic data for **1**–**4** are listed in Table 2 and selected bond lengths and angles are given in Table 3. Further details of the crystal structure investigation can be obtained from the Fachinformationzentrum Karlsruhe, 76344 Eggenstein-Leopoldshafen, Germany, on quoting the depository number CSD-417040, -417038, -417039, and -417037 for **1**–**4**, respectively.

Computational Details: The X-ray crystallographic data of the present compounds were used to calculate their electronic band structures. The calculations of electronic band structures along with density of states (DOS) were carried out using density functional theory (DFT) with one of the three nonlocal gradient-corrected exchange-correlation functionals (GGA-PBE) and performed with the CASTEP code,[13] which uses a plane wave basis set for the valence electrons and norm-conserving pseudopotential[14] for the core electrons. The number of plane waves included in the basis was determined by a cutoff energy, E_c, of 450 eV for **1**, **3**, and **4**, and 400 eV for **2**. Pseudo-atomic calculations were performed for Cl $3s^23p^5$, Br $4s^24p^5$, I $5s^25p^5$, As $4s^24p^3$, Sb $5s^25p^3$, Cd $4d^{10}5s^2$, and Hg $5d^{10}6s^2$. The parameters used in the calculations and convergence criteria were set by the default values of the CASTEP code.[13]

Supporting Information: (see also the footnote on the first page of this article): Experimental and simulated powder X-ray diffraction patterns, TG and DTA curves, and IR spectra of compounds **1**–**4**.

Acknowledgments

We gratefully acknowledge the financial support of the National Science Foundation of China (20571075 and 20521101), the National Science Foundation for Distinguished Young Scientists of China (20425104), and the National Science Foundation of CAS (KJCX2-SW-h05).

[1] a) G. R. Desiraju, *Angew. Chem. Int. Ed. Engl.* **1995**, *34*, 2311–2327; b) A. Müller, H. Reuter, S. Dillinger, *Angew. Chem. Int. Ed. Engl.* **1995**, *34*, 2328–2361.

[2] a) A. V. Olenev, A. I. Baranov, O. S. Oleneva, I. I. Vorontsov, M. Y. Antipin, A. V. Shevelkov, *Eur. J. Inorg. Chem.* **2003**, 1053–1057; b) A. V. Olenev, O. S. Oleneva, M. Lindsjö, L. A. Kloo, A. V. Shevelkov, *Chem. Eur. J.* **2003**, *9*, 3201–3208; c) O. S. Oleneva, A. V. Olenev, E. V. Dikarev, A. V. Shevelkov, *Eur. J. Inorg. Chem.* **2004**, 4006–4010; d) A. V. Olenev, A. I. Baranov, A. V. Shevelkov, B. A. Popovkin, *Eur. J. Inorg. Chem.* **2002**, 547–553; e) J.-P. Zou, G.-C. Guo, W.-T. Chen, X. Liu, M.-L. Fu, Z.-J. Zhang, J.-S. Huang, *Inorg. Chem.* **2006**, *45*, 6365–6369; f) A. V. Shevelkov, M. M. Shatruk, *Russ. Chem. Bull. Int. Ed.* **2001**, *50*, 337–362; g) A. V. Olenev, A. V. Shevelkov, *Angew. Chem. Int. Ed.* **2001**, *40*, 2353–2354; h) A. V. Olenev, A. I. Baranov, A. V. Shevelkov, B. A. Popovkin, *Eur. J. Inorg. Chem.* **2000**, 265–270.

[3] a) A. V. Shevelkov, E. V. Dikarev, M. Yu. Mustiakimov, B. A. Popovkin, *J. Chem. Soc., Dalton Trans.* **1996**, 147–148; b) A. V. Shevelkov, E. V. Dikarev, B. A. Popovkin, *J. Solid State Chem.* **1996**, *126*, 324–327; c) A. V. Olenev, A. V. Shevelkov, B. A. Popovkin, *Russ. J. Inorg. Chem.* **1999**, *44*, 1814–1816; d) A. V. Olenev, A. V. Shevelkov, B. A. Popovkin, *Russ. J. Inorg. Chem.* **1999**, *44*, 1853–1861; e) J. Beck, U. Neisel, *Z. Anorg. Allg. Chem.* **2000**, *626*, 1620–1626; f) J. Beck, S. Hedderich, U. Neisel, *J. Solid State Chem.* **2000**, *154*, 350–355; g) $(Hg_2As)_2(CdI_4)$: J.-P. Zou, D.-S. Wu, S.-P. Huang, J. Zhu, G.-C. Guo, J.-S. Huang, *J. Solid State Chem.*, DOI: 10.1016/j.jssc.2006.11.018.

[4] a) L. Nijssen, W. N. Lipscomb, *Acta Crystallogr.* **1954**, *7*, 103–106; b) W. R. Dorff, K. Brodersen, *Z. Anorg. Allg. Chem.* **1953**, *274*, 323–340; c) R. Airoldi, G. Magnano, *Rass. Chim.* **1967**, *5*, 181–189.

[5] a) H. Puff, M. Grönke, B. Kilger, P. Möltgen, *Z. Anorg. Allg. Chem.* **1984**, *518*, 120–124; b) A. V. Shevelkov, M. M. Shatruk, *Russ. Chem. Bull. Int. Ed.* **2001**, *50*, 337–362.

[6] a) A. V. Shevelkov, E. V. Dikarev, B. A. Popovkin, *J. Solid State Chem.* **1992**, *98*, 133–136; b) A. V. Shevelkov, E. V. Dikarev, B. A. Popovkin, *J. Solid State Chem.* **1993**, *104*, 177–180.

[7] a) R. Laiho, A. V. Lashkul, K. G. Lisunov, E. Lähderanta, M. O. Safonchik, M. A. Shakhov, *J. Phys. Condens. Matter* **2004**, *16*, 333–342; b) R. Laiho, A. V. Lashkul, K. G. Lisunov, E. Lähderanta, M. O. Safonchik, M. A. Shakhov, *Semicond. Sci. Technol.* **2004**, *19*, 602–609.

[8] a) G. A. Mousdis, V. Gionis, G. C. Papavassiliou, C. P. Raptopoulou, A. Terzis, *J. Mater. Chem.* **1998**, *8*, 2259–2262; b) M. Braum, W. Tuffentsammer, H. Wachtel, H. C. Wolf, *Chem. Phys. Lett.* **1999**, *307*, 373–378.

[9] a) C. H. Champness, *Phosphorus, Sulfur Relat. Elem.* **1988**, *38*, 385–397; b) R. H. Dube, *Photovoltaic Materials*, Imperial College Press, **1998**, p. 135; c) P. Dürichen, W. Bensch, *Eur. J. Solid State Inorg. Chem.* **1997**, *34*, 1187–1190.

[10] a) J. A. Harrington, *Infrared Fibers and Their Applications*, SPIE Press, Bellingham, WA, **2004**; b) D. Marchese, M. De Sario, A. Jha, A. K. Kar, E. C. Smith, *J. Opt. Soc. Am. B* **1998**, *15*, 2361–2370.

[11] a) W. W. Wendlandt, H. G. Hecht, *Reflectance Spectroscopy*, Interscience Publishers, New York, **1966**; b) G. Kortüm, *Reflectance Spectroscopy*, Springer-Verlag, New York, **1969**.

[12] *Siemens SHELXTL™ Version 5 Reference Manual*, Siemens Energy & Automation Inc., Madison, Wisconsin, U. S. A. **1994**.

[13] a) M. Segall, P. Linda, M. Probert, C. Pickard, P. Hasnip, S. Clark, M. Payne, *Materials Studio CASTEP version 2.2*, **2002**; b) M. Segall, P. Linda, M. Probert, C. Pickard, P. Hasnip, S. Clark, M. Payne, *J. Phys.: Condens. Matter* **2002**, *14*, 2717–2744.

[14] D. R. Hamann, M. Schluter, C. Chiang, *Phys. Rev. Lett.* **1979**, *43*, 1494–1797.

Received: September 25, 2006
Published Online: January 16, 2007

